An efficient bifunctional Ni-Nb_2O_5 nanocatalysts for the hydrodeoxygenation of anisole

Juan Xu,[a,b] Ping Zhu,[c] Islam H. El Azab,[d] Ben Bin Xu,[e] Zhanhu Guo,[f,*] Ashraf Y. Elnaggar,[d] Gaber A.M. Mersal,[g] Xiangyi Liu,[b] Yunfei Zhi,[a] Zhiping Lin,[h] Hassan Algadi,[i] and Shaoyun Shan[a,*]

[a] Faculty of Chemical Engineering, Kunming University of Science and Technology, Kunming, 650500, China

[b] College of Chemical Engineering, Southwest Forestry University, Kunming 650224, China

[c] Yunnan Province Special Equipment Safety Inspection and Research Institute, Kunming 650228, China

[d] Department of Food Science and Nutrition, College of Science, Taif University, Taif 21944, P. O. Box 11099, Saudi Arabia.

[e] Department of Mechanical and Construction Engineering, Faculty of Engineering and Environment, Northumbria University, Newcastle upon Tyne, NE1 8ST, UK

[f] Integrated Composites Lab (ICL), Department of Chemical & Biomolecular Engineering, University of Tennessee, Knoxville, TN 37996, USA

[g] Department of Chemistry, College of Science, Taif University, P.O. Box 11099, Taif 21944, Saudi Arabia.

[h] Taizhou University, No. 1139, Shifu Road, Taizhou, 31800 China

[i] Department of Electrical Engineering, Faculty of Engineering, Najran University, P.O. Box 1988, Najran 11001, Kingdom of Saudi Arabia

*: Corresponding author

E-mail: shansy411@163.com (S. Shan);

nanomaterials2000@gmail.com (Z. Guo)

Abstract

The Ni-Nb_2O_5 nanocatalysts have been prepared by the sol-gel method, and the catalytic hydrodeoxygenation (HDO) performance of anisole as model compound is studied. The results show that Nb exists as amorphous Nb_2O_5 species, which can promote Ni dispersion. The addition of Nb_2O_5 increases the acidity of the catalyst. However, when the content of niobium is high, there is an inactive Nb-Ni-O mixed phase. The size and morphology of Ni grains in catalysts are different due to the difference of Nb/Ni molar ratio. The $Ni_{0.9}Nb_{0.1}$ sample has the largest surface area of 170.8 $m^2 \cdot g^{-1}$ among the catalysts prepared in different Nb/Ni molar ratios, which is mainly composed of spherical nanoparticles and crack pores. The HDO of anisole follows the reaction route of the hydrogenation HYD route. The $Ni_{0.9}Nb_{0.1}$ catalyst displayed a higher HDO performance for anisole than Ni catalyst. The selectivity to cyclohexane over the $Ni_{0.9}Nb_{0.1}$ sample is about 10 times that of Ni catalyst at 220 ℃ and 3 MPa H_2. The selectivity of cyclohexane is increased with the increase of reaction temperature. The anisole is almost completely transformed into cyclohexane at 240℃, 3 MPa H_2 and 4 h.

Keywords: Hydrodeoxygenation (HDO) · catalysts · Ni-Nb_2O_5 · sol-gel method · Anisole

1. Introduction

Under the dual pressure of energy shortage [1-13] and environmental deterioration [14-29], the safe environmentally friendly and renewable fuels like hydrogen [30,32], biofuel, *et al*. are pursued [32-35]. Exploiting nature's abundant renewable carbon resources in nature can reduce society's dependence on non-renewable fossil fuel reserves [36-38]. Biomass is a rich renewable carbon resource [39-40]. Biomass can be used in many ways, such as direct combustion, straw returning to the field, compression molding, composting to produce biogas fertilizer, etc. [41-44]. However, these forms of utilization are low efficiency and one-dimensional. Researchers have found that bio-oil

produced by pyrolysis can be used as an alternative fuel for gasoline and diesel for the past few years，and can also reduce carbon dioxide emissions and promote carbon neutrality [43,45]. Bio-oil has a great development potential and will become an important part of energy in the future [46]. But bio-oil contains high oxygen content (40% ~ 50% by mass fraction), and is composed of phenols, esters, furans, ketones and other compounds. Compared with traditional fossil energy, bio-oil has many problems, such as very complex chemical composition, high oxygen content, unstable properties, low acid value, low calorific value, corrosive to equipment and so on [47-48]. So it should not be used directly (e.g. as fuel) before its quality upgrade is further improved [49].

Hydrodeoxidation (HDO) is one of the important methods to improve the quality of bio-oil, and includes two aspects: hydrogenation and deoxygenation. The calorific value of bio-oil is increased by reducing oxygen content and saturating most aromatic compounds and alkenes [50]. Catalytic hydrodeoxidation (CHDO) is to remove oxygen selectively from bio-oil under mild reaction conditions by adding efficient catalysts, so as to obtain higher purity fuels or chemicals. Recently, CHDO has become a hot topic in the field of biomass energy, especially the mechanism of CHDO and the preparation of the efficient catalyst. The mechanism of CHDO was studied mainly through model compounds of bio-oil, including the relationship between the structure of catalyst and hydrodeoxidation performance of model compounds, and the reaction pathway of model compounds were discussed. Frequently, selected model compounds contain aldehydes (-CO), methoxyl (-OCH_3) and phenolic hydroxyl (-OH) groups such as phenol, anisole, cresol, guaiphenol, vanillin and so on. Related studies show that the main ways of hydrodeoxidation of model compounds are HYD (hydrogenation), DDO (direct deoxidation), TMA (methyl transfer) and so on [51-53].

Many kinds of catalysts have been researched for CHDO, including precious metals

[54,55], transition metal [56-58],metal carbide [59], metal phosphates [60] and bifunctional catalysts [53]. Bifunction catalysts contain two types of catalytic active centers: metal center and acid center. The metal center is the active center for hydrogenation sites, while the acid center is the active center for deoxygenation sites. They can convert oxygenated compounds directly into alkanes. Among hydrogenated metals, Ni is relatively cheap compared with precious metals, and is considered to be a very effective species, with high activity, no pollution, not easy to be deactivated and other advantages [61]. The effective combination of acidic site with hydrogenated metals can enhance HDO activity. Acidic materials are used to provide acidic sites, such as acidic molecular sieve, ZrO_2, Al_2O_3, TiO_2 and other acidic materials have been widely used to construct dual-function deoxidation catalysts [62-63]. However, the water generated by hydrodeoxygenation will poison the surface acidity of the solid acid and lead to the deactivation of the catalyst.

Niobium containing materials with both Bronsted and Lewis acid sites have attracted extensive attention in the solid acid catalyst field because of their good water resistance and thermal stability [64], and can easily catalyzed esterification, hydrolysis and other important reactions, so they are widely used in organic synthesis [65]. In addition, bifunctional catalysts constructed from niobium materials have been successfully applied in field of biomass catalytic conversion. For example, Nb_2O_5 is used for the deoxidation of fatty acids, and sorbitol is converted into hexane by $NbOPO_4$, achieving better deoxidation effects [66]. Although, in previous work, there were many reports on the advantages of bifunctional catalysts constructed by niobium-based materials and precious metals for bio-oil, such as good catalytic performance, stability and high selectivity [67], there were few reports on the efficient hydrocarbon production of bifunctional catalysts constructed by niobium based materials and transition metals

instead of precious metals in bio-oil system.

In this study, a kind of bifunctional Ni-Nb_2O_5 catalyst was designed by sol-gel method for the hydrodeoxidation of anisole. The morphology and structure of the catalyst were analyzed, and the effects of reaction conditions on hydrodeoxidation performance were investigated. Nb/Ni ratios had a greater influence on the structure and catalytic activity of catalysts. After this, the stability of Ni-Nb_2O_5 was further studied, and the catalytic reaction pathway of anisole was proposed.

2. Experimental

2.1 Catalyst Preparation

Unsupported NiNbO composite oxide precursor was prepared by the sol-gel method and then Ni-Nb catalyst was obtained by hydrogen reduction. The process can be briefly stated as follows: 10 mmol citric acid (1.92 g) and a certain amount of $Ni(NO_3)_2$▪$6H_2O$ was dissolved in 20 mL of 80% ethanol solution, denoted as solution 1. A certain amount of niobium (V) oxalate hydrate was dissolved in 10 mL water, denoted as solution Ⅱ. Then solution Ⅰ and solution Ⅱ were mixed evenly, denoted as solution Ⅲ, where the molar mass of (Ni+Nb) was 10 mmol, of which Nb was 0.05 mmol, 0.1 mmol, 0.2 mmol and 0.3 mmol, respectively. The mixture was heated and evaporated in a water bath at 80℃, and the complex was polymerized to form viscous colloid. Then, the wet gel was obtained by ultrasound for 15 min. The xerogel was obtained by drying wet gel at 110 ℃ for one hour, and programmed calcine (heating procedure: 2℃·min^{-1} to 180℃ for 2h, and then 5 ℃·min^{-1} to 500℃ for 5h) to obtain the unsupported Ni-Nb-O composite oxide precursor, which is expressed as $Ni_{1-x}Nb_xO$ (x=0.05,0.1,0.2,0.3). Finally, it was placed in the tube furnace for reduction under 450℃ for 5 h in 10 %(vol) H_2/Ar atmosphere, to get the Ni-Nb catalyst, denoted as $Ni_{1-x}Nb_x$.

2.2 Characterization of Catalysts

The X-ray powder diffraction (XRD), transmission electron microscopy (TEM), scanning electron microscope (SEM), NH_3-TPD, X-ray photoelectron spectroscopy (XPS) and N_2 adsorption-desorption analysis were used to characterize the powdered catalysts. A JEOL JE-2100 electron microscope at 200 kV acceleration voltage was used to obtain TEM images. The N_2 physical adsorption-desorption measurement was conducted with Kanta nova1200e instrument. The BET surface, pore volume and pore size distribution were estimated through Barrett-Joyner-Halenda (BJH) models. XPS analysis were investigated by employing an ESCALAB250XL (Thermo VG, USA) spectrometer. NH_3-TPD analysis and H_2-TPR analysis were performed on an AutoChem1 Ⅱ 2920 analyzer. The SEM (Nova450 from FEI Co.) and energy dispersive X-ray (EDX) analyzer were used to analyze and characterize the morphology and structural composition of the catalysts.

2.3 Catalytic Activity Tests

Using anisole, a typical oxygen-containing compound of bio-oil, as raw material, the catalytic hydrodeoxygenation reactions were carried out in a 50 mL stainless steel reactor (Beijing Shiji Senlang Experimental Instrument Co., Ltd). Typically, catalyst (0.1 g) and anisole (13.9 mmol) were loaded into an autoclave reactor with n-dodecane (15 mL) as the solvent. First, Ar gas was passed into the reactor to replace the air three times to exhaust the air in the kettle. Then, hydrogen was introduced to replace the argon gas in the reactor twice. Subsequently, hydrogen was filled with the set pressure (1-3 MPa), the stirring speed was adjusted to 700 RPM, the reaction temperature was set in the range of 200-250℃, and the reaction temperature was maintained for a period of time (1-6 h). After the reaction was completed according to the set time, the reactor was cooled down to room temperature, and the products were removed and filtered through a 0.22um nylon filter, and then analyzed.

2.4 Product Analysis

GC/MS (Agilent 7890A/5975C) was used for qualitative analysis of the product, with HP-5 MS column (50 m × 0. 25 mm × 0.25 μm). The temperatures of the injection port and detector were 260℃ and 280 ℃, respectively. The heating program was that the initial column temperature was set at 40℃ for 2 min, and then heated to 240℃ at a rate of 20 ℃·min^{-1} for 5 min. The quantitative analysis of the products was implemented by gas chromatography (GC, Agilent 7890, FID), and the chromatographic column was HP-5 column. The conversion of reactant, the selectivity and yield of products were calculated by Eqs. (1–3):

$$Conversion(\%) = (anisole^{in} - anisole^{out})/anisole^{in} \times 100 \quad (1)$$

$$Selectivity(\%) = \frac{produced\ moles\ of\ \ specific\ component}{consumed\ moles\ of\ anisole} \times 100 \quad (2)$$

$$Yield(\%) = Conversion(\%) \times Selectivity(\%)/100 \quad (3)$$

3. Results and Discussion

3.1 Catalyst characterization

(1) XRD

Fig.1(a) shows the XRD patterns of $Ni_xNb_{1-x}O$ mixed oxide precursor after calcination. All the $Ni_xNb_{1-x}O$ oxide samples showed the (111), (200), (220), (311) and (222) typical reflections of NiO (JCPDS 89-7130), close to 2θ =37.2°, 43.2°, 63.0°, 75.2°and 79.2°. As the amount of Nb in the sample is increased, a low-intensity and wide-range background peak (local magnification) at around 26° is ascribed to the amorphous niobium oxides [68]. $Ni_{0.7}Nb_{0.3}O$ sample shows the peaks at 2θ of 35.2°, 40.8°, and 53.5°, which are attributed to the mixed phase of Ni-Nb-O [69]. It was reported that when Nb in the sample is low, niobium is mainly in the form of amorphous Nb_2O_5 phase, but when Nb in the sample is high, it will form the mixed phase of Ni-Nb-O (e.g. $NiNb_2O_6$, $Ni_3Nb_2O_8$, etc.).The presence of the mixed phase results in a reduced catalytic activity [70,71].In addition, the hydrated niobic acid ($Nb_2O_5·H_2O$) only showed

amorphous broad peaks and did not transform into crystalline Nb_2O_5 after calcination at 500℃.

According to Fig.1(b), all Ni-Nb samples showed the characteristic peaks of Ni crystal phase after hydrogenation (PDF04-0850). The diffraction peaks at 44.5°, 51.8° and 76.5° correspond to the (111), (200) and (220) crystal faces of Ni, respectively. However, there is also the mixed phase of Ni-Nb-O in the sample of $Ni_{0.7}Nb_{0.3}$, indicating that the mixing is relatively stable and not easy to be reduced.

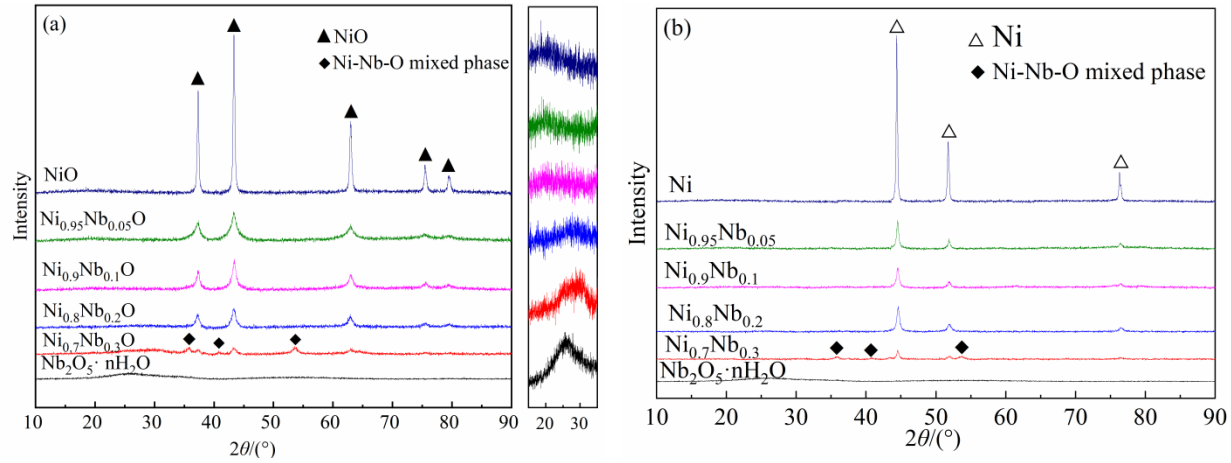

Fig. 1 (a) XRD patterns of $Ni_xNb_{1-x}O$ mixed oxide precursor after calcination. (b) XRD patterns of Ni_xNb_{1-x} catalyst after reduction.

(2) N_2 adsorption-desorption analysis

The suitable pore structure is one of the important factors for the bulk catalysts to provide a catalytic reaction activity. The total pore volume (PV), average pore size (PS), crystallite size (CS) and specific surface area (SA) of the $Ni_{1-x}Nb_x$ catalysts with different proportions are shown in Table 1.

Table 1. Physicochemical performances of $Ni_{1-x}Nb_x$

Catalyst	BET surface(SA)[a] /$m^2 \cdot g^{-1}$	Pore size(PS)[a] /nm	Pore volume(PV)[a] /$cm^3 \cdot g^{-1}$	Crystallite size(CS)[b] /nm
Ni	67.9	6.3	0.11	23.7
$Ni_{0.95}Nb_{0.05}$	161.3	3.1	0.24	15.3
$Ni_{0.9}Nb_{0.1}$	170.8	4.7	0.37	13.2
$Ni_{0.8}Nb_{0.2}$	93.1	8.6	0.15	16.1
$Ni_{0.7}Nb_{0.3}$	70.8	9.2	0.12	18.8
$Nb_2O_5 \cdot H_2O$	102.4	5.1	0.20	-

[a] From N_2 adsorption measurements (BJH method), Pore size= the average diameter of pore.

[b] Determined considering the Ni(111) peak higher intensity

It is seen that in catalysts with a low niobium content, the non-crystal phase of Nb_2O_5 can promote the dispersion of Ni to increase the specific surface area. When the Ni/Nb molar ratio was 0.9/0.1, the SA and PV reached 170.8 $m^2 \cdot g^{-1}$ and 0.37 $cm^3 \cdot g^{-1}$, respectively. With the increase of niobium in sample, the SA and PV of catalyst are gradually decreased, which may be due to the increase of niobium content and nickel reaction to generate the inactive Ni-Nb-O mixture phase, and easy to reunite the catalyst grains and the grain size becomes larger. In addition, the nickel crystallite size of different proportional $Ni_{1-x}Nb_x$ samples calculated by Scherrer formula is displayed in Table 1. It indicates an inverse relationship between the nickel crystallite size and the corresponding surface area.

(3) XPS

Three more typical samples of NiO, $Ni_{0.9}Nb_{0.1}O$, and $Ni_{0.7}Nb_{0.3}O$ were selected for x-ray photoelectron spectroscopy (XPS) tests, as shown in Fig.2. The two main peaks of Ni $2p_{3/2}$ close to 854.2 and 856.0 eV belong to Ni^{2+} and Ni^{3+} species, respectively [72]. When the niobium content is added in the sample, the peak area ratio of Ni^{2+}/Ni^{3+} increases, possibly because that the Ni^{3+} species is gradually consumed by Nb to form the Ni-Nb-O mixing phase [69]. On the other hand, the main peak Nb $3d_{5/2}$ of the XPS spectrum Nb 3d (Fig.2(b)) is 206.7 ev, and the binding energy of niobium species

matches well with that of Nb^{5+} [73], indicating that Nb in the sample is in the highest oxidation state (i.e. +5 valence).

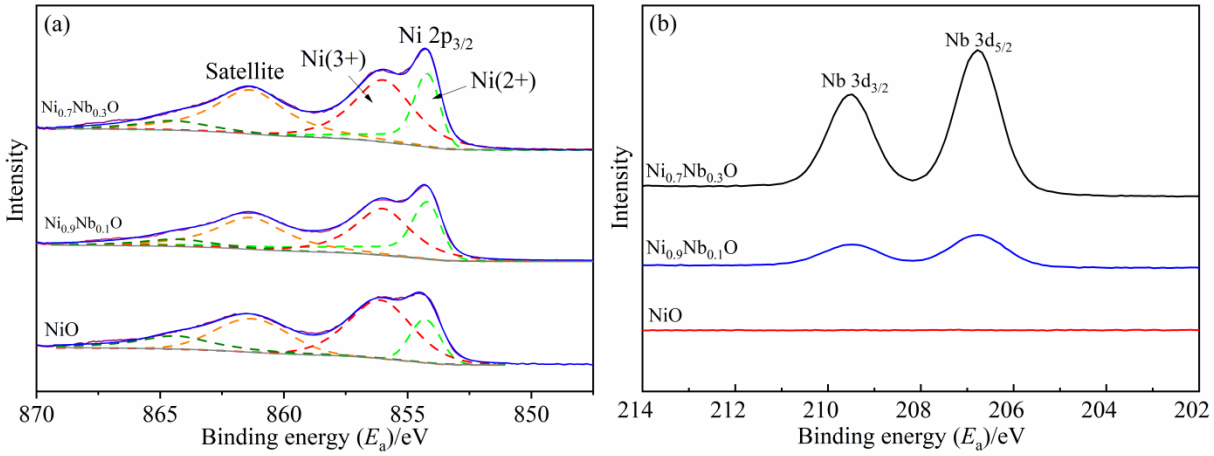

Fig.2 XPS spectra of NiO, $Ni_{0.9}Nb_{0.1}O$ and $Ni_{0.7}Nb_{0.3}O$ samples (a) Ni 2p3/2 and (b) Nb 3d.

The Ni 2p3/2 spectra of the reduced samples (Ni, $Ni_{0.9}Nb_{0.1}$, and $Ni_{0.7}Nb_{0.3}$) were examined by XPS with the profiles presented in Fig.3. As shown in Fig.3 (a), the Ni 2p3/2 region has three peaks at about 852.4, 855.5 and 860.7 eV respectively, which are related to Ni^0, Ni^{2+} and Ni^{2+} shakeup satellite peaks [56,57]. Meanwhile, we noticed that the binding energy of Ni^0 species is decreased with the introduction of Nb, from 852.4 eV to 852.2 eV, indicating that the addition of Nb would increase the density of Ni^0 electron cloud. In addition, there were a large number of Ni^{2+} species on the surface of each reduction sample, and the surface fraction of Ni^0 species in the total Ni species is decreased with the introduction of Nb. On the other hand, the binding energy of niobium species after reduction (206.7eV) matches that of Nb^{5+}, which is consistent with that of Nb species before reduction, indicating that Nb species is still in the highest oxidation state (i.e. +5 valence).

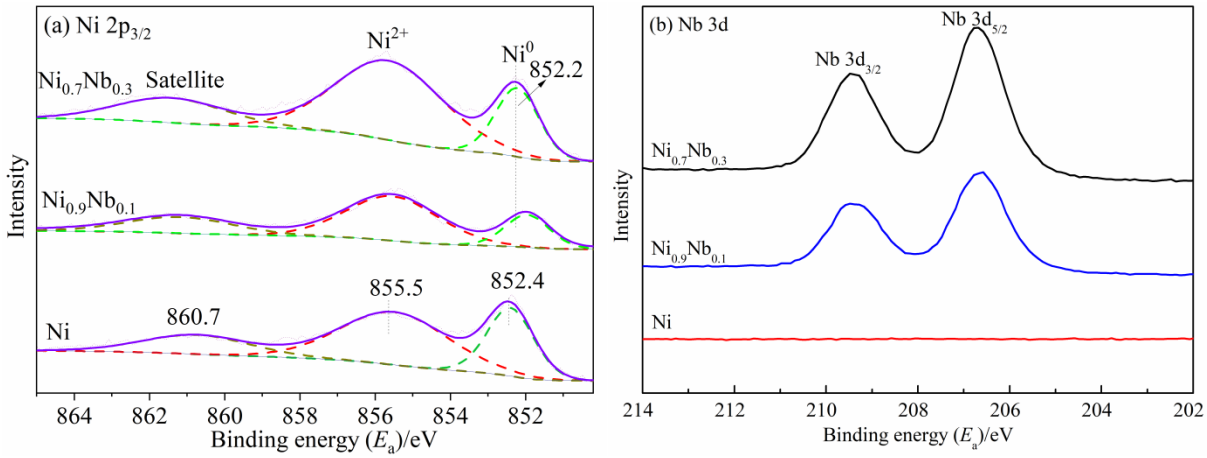

Fig.3 XPS spectra of Ni, $Ni_{0.9}Nb_{0.1}$ and $Ni_{0.7}Nb_{0.3}$ samples (a) Ni 2p3/2 and (b) Nb 3d

(4) NH_3-TPD

The acidity of the samples was measured by the thermo-programmed desorption of ammonia (TPD-NH_3). The profiles of Ni, $Ni_{0.9}Nb_{0.1}$ and $Ni_{0.7}Nb_{0.3}$ catalysts are presented in Fig.4. According to the desorption peak temperature, the solid surface acid strength can be segmented into strong acid (above 450 ℃), medium strong acid (250-350 ℃) and weak acid (150-250 ℃) [74]. Two main desorption peaks of NH_3 are observed for Ni0.9Nb0.1, located at 205 ℃ and 444 ℃, respectively, with the former representing the weak acid site and the latter representing the medium strong acid site [75]. According to relevant studies, the acid concentration of catalyst can be reflected by the area of the peak [76]. The area of desorption peak (total acid content) follows: $Ni_{0.9}Nb_{0.1}$＞$Ni_{0.7}Nb_{0.3}$ ＞Ni, which indicates that the addition of niobium species enhances the acidity of the sample. $Ni_{0.7}Nb_{0.3}$ may be due to the existence of the inert mixed phase (Ni-Nb-O), resulting in a weak acid strength.

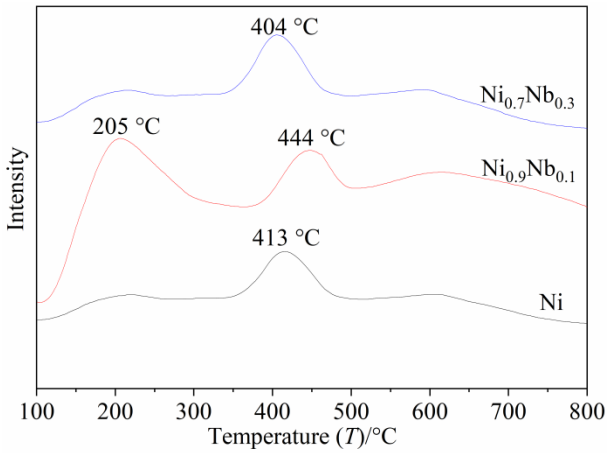

Fig.4 NH_3-TPD profiles of Ni, $Ni_{0.9}Nb_{0.1}$ and $Ni_{0.7}Nb_{0.3}$ catalysts.

(5) H_2-TPR

The H_2-TPR profiles of three typical NixNb1-xO mixed oxide samples (NiO, $Ni_{0.9}Nb_{0.1}O$ and $Ni_{0.7}Nb_{0.3}O$) are displayed in Fig.5. The TPR curve of bulk nickel oxide shows a reduction peak at around 450 ℃, which is caused by the $Ni^{2+} \rightarrow Ni^0$ reduction step. With the increase of niobium content, the reduction peak moves towards a high temperature, indicating that the interaction between nickel and niobium oxide is enhanced.

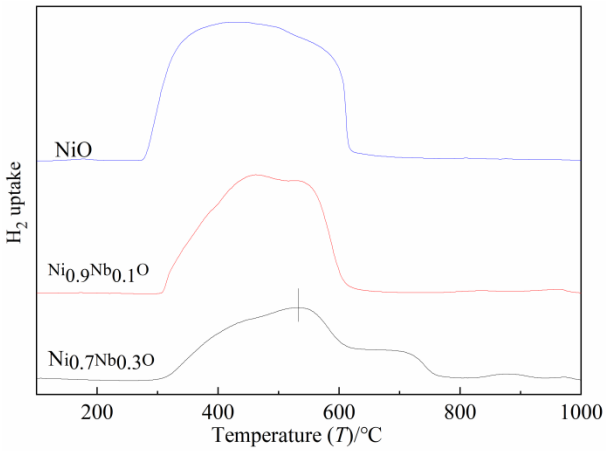

Fig.5 H_2-TPR profiles of NiO, $Ni_{0.9}Nb_{0.1}O$ and $Ni_{0.7}Nb_{0.3}O$ catalysts.

(6) SEM

The surface morphology of the prepared catalyst was detected by scanning electron microscope (SEM). The micrographs of $Ni_{0.9}Nb_{0.1}$, $Ni_{0.7}Nb_{0.3}$ and pure Ni are shown in Fig.6(A). It shows that the pure Ni catalyst surface layer of the bulk phase is relatively

dense with an irregular porous structure. The surface layer of $Ni_{0.9}Nb_{0.1}$ sample is relatively loose, showing uniform spherical nanoparticles and crack holes, with regular arrangement. The arrangement of loose surface particles facilitates the diffusion of reactants to the active center, thus improving the catalytic activity. The morphology changed obviously with the increasement of Nb, the spherical nanoparticles and pore structure were found in the $Ni_{0.7}Nb_{0.3}$ sample.

The distribution of niobium species in the bulk phase Ni catalyst was obtained by the X-ray maps and the Nb/Ni mole ratio of the catalyst surface was tested by the EDX, as shown in Fig.6(B). It is obvious that niobium species in the sample are evenly distributed, indicating that a homogeneous Ni-Nb catalyst can be prepared by the sol-gel method. Besides, the Nb/Ni mole ratio on the surface of $Ni_{0.9}Nb_{0.1}$ sample was 0.12/0.9 according to the EDX test, slightly above the calculated values of 0.1/0.9, which demonstrates that the $Ni_{0.9}Nb_{0.1}$ sample was enriched with niobium on the surface.

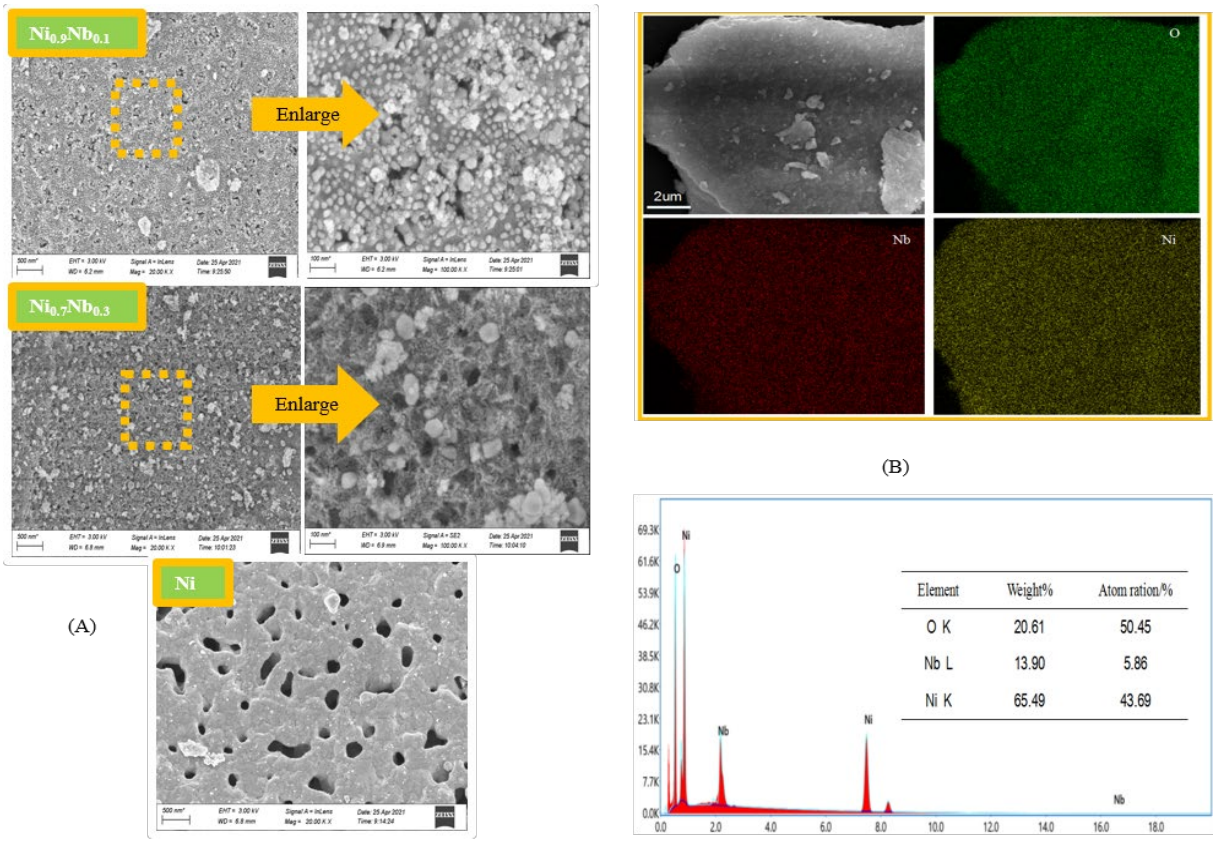

Fig. 6 (A) SEM images of Ni-Nb and Ni, (B)X-ray maps of Ni, Nb and EDX results of $Ni_{0.9}Nb_{0.1}$ sample.

(6) TEM

A high-resolution transmission electron (TEM) image of the reduced $Ni_{0.9}Nb_{0.1}$ catalyst sample is displayed in Fig.7. It indicates that metal nickel nanoparticles are evenly distributed, and there are a few amorphous structures probably because of the non-crystal niobium oxides. The lattice fringe of the Ni crystal phase is observed in Fig.5(c), and the lattice spacing of the metallic Ni calculated by two-dimensional Fast Fourier transform (FFT) is 0.204 nm, corresponding to the (111) plane of Ni. The particle size distribution of nanosphere composites is shown in Figure 5(d). It can be seen that the particle size of $Ni_{0.9}Nb_{0.1}$ is in the range of 10-14 nm, and the average particle size is 12.9 nm, which is close to the grain size calculated by XRD data (13.2 nm).

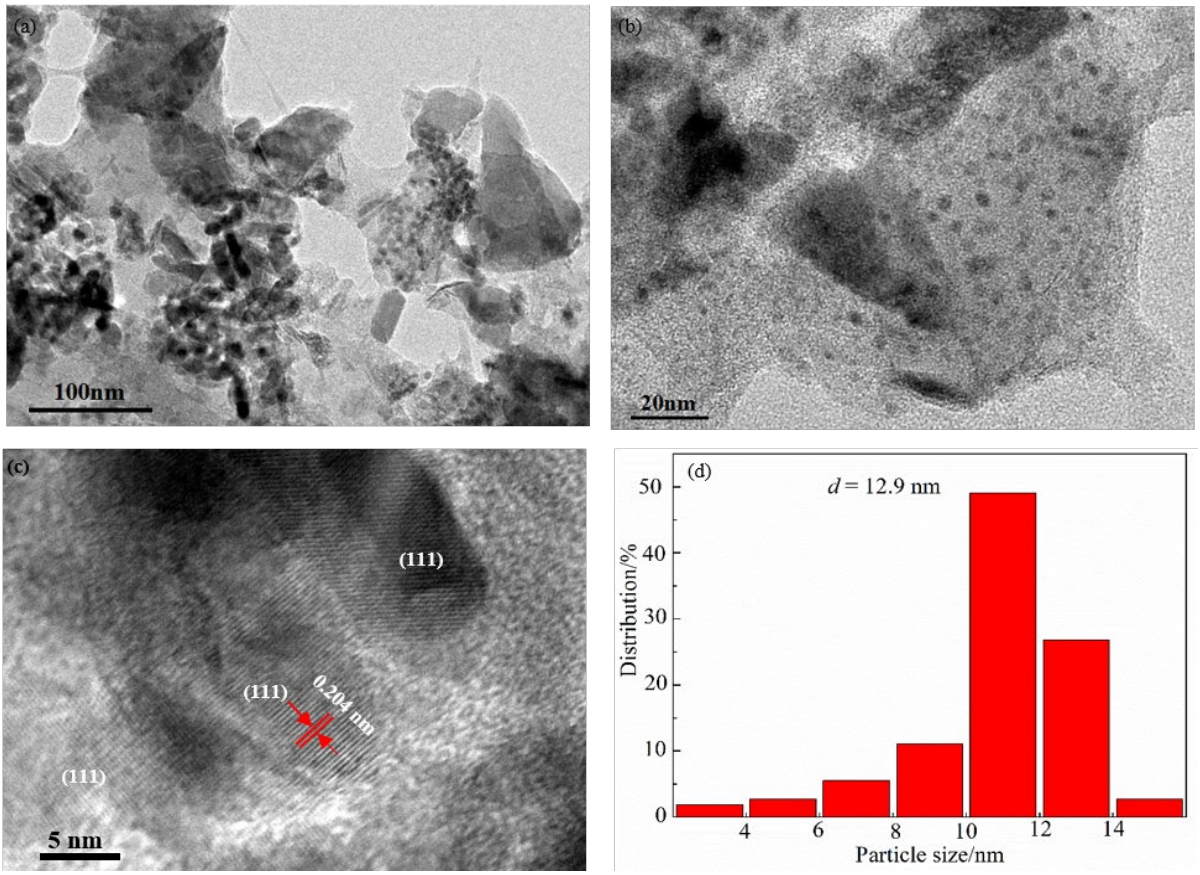

Fig.7. (a-c) TEM images and (d) the particle size distribution histogram of $Ni_{0.9}Nb_{0.1}$.

3.2 Catalytic hydroconversion of anisole

To initially discuss the hydrodeoxygenation performance of the Ni_xNb_{1-x} catalysts with different Ni/Nb molar ratios, the hydrodeoxidation (HDO) test of anisol, a model compound of biological oil, was carried out in a high pressure reactor at 220 ℃ and 3

MPa H_2 pressure. The conversion of reactants and selectivity of products over Ni_xNb_{1-x} samples with different Nb/Ni molar ratios are shown in Table 2. Methoxy cyclohexane (MCH), cyclohexane (CHN) and cyclohexanol (CHL) were the main products from CHDO of anisole, which were tested by GC-MS.

Table 2. Hydrodeoxygenation of anisole over Ni_xNb_{1-x} catalysts

Catalyst	Selectivity/%			Conversion/ %	R_{rate}[a]/mmol·g^{-1}·h^{-1}
	cyclohexane	cyclohexanol	methoxyclohexane		
Ni	8.1	41.1	50.8	72.3	25.1
$Ni_{0.95}Nb_{0.05}$	76.8	3.1	20.1	97.8	34.0
$Ni_{0.9}Nb_{0.1}$	79.2	1.8	19.0	99.6	34.6
$Ni_{0.8}Nb_{0.2}$	52.1	10.7	37.2	84.6	29.4
$Ni_{0.7}Nb_{0.3}$	48	18.5	33.5	79.8	27.7
$Nb_2O_5·H_2O$	-	-	-	0	-

Reaction conditions: 0.1g Ni_xNb_{1-x} catalyst,13.9mmol anisole,15mLC_{12},220℃，3MPa,4h,700rpm
[a]R_{rate}=mmol(converted anisole/[g(catalyst amount)×h(time)].

The conversion of anisole is 72.3% and the selectivity of methoxycyclohexane is 50.8% after 4-hour hydrogenation on bulk Ni catalyst. However, the selectivity of cyclohexane is only 8.1%, and the poor deoxidation performance of bulk Ni as a catalyst may be due to the weak acidity of nickel [77]. The conversion of reactant and the deoxidization performance of the catalyst were significantly improved after the addition of niobium, which may be related to the fact that amorphous Nb_2O_5 can provide acid active sites for hydrodeoxidation [70,78]. Among them, the $Ni_{0.9}Nb_{0.1}$ sample showed the highest hydrodeoxygenation, with a conversion rate of 99.6% and a selectivity of cyclohexane of 79.2%. The conversion rate (Rrate) (34.6 mmol·g^{-1}·h^{-1}) of the $Ni_{0.9}Nb_{0.1}$ catalyst was 1.4 times that of the ordinary Ni catalyst, and the selectivity of deoxidation product was about 10 times that of ordinary Ni catalyst. However, when the content of Nb in the catalyst was high (e.g., $Ni_{0.7}Nb_{0.3}$), the deoxidation activity was decreased due to the formation of the inert Nb-Ni-O mixture phase [79]. In addition, the $Nb_2O_5·H_2O$ was also used for the HDO of anisole, but it did not show any reactivity. Therefore, it can be concluded that the good hydrogenation and deoxidation performance of bifunctional $Ni_{1-x}Nb_x$ catalysts is due to the synergistic effect of metal and acid sites.

Considering that $Ni_{0.9}Nb_{0.1}$ catalyst has the best hydrodeoxidation performance

compared with other three catalysts in different proportions, thus it was used to discuss the distribution of the products from HDO of anisole under different reaction conditions, which is shown in Fig.8 and Fig.9.

The bar chart shows the selectivity of product and the line chart shows the conversion of anisole in Fig.8. From Fig.8(a), under different reaction pressures, the conversion of reactants and the selectivity of products changed obviously. The conversion rate from HDO of anisole was increased from 65.8% to 99.0% with the increase of reaction pressure from 1 to 3 MPa. The hydrogenation and subsequent deoxidation of aromatic ring in anisole occur more easily at 3.0 MPa, and the selectivity of cyclohexane is increased from 36.8 to 79.2%. According to Fig.8(b), the raw material anisole can be completely transformed in the range of 200-240 ℃, and the conversion rate is over 92%. Hydrogenation of aromatic ring is a fast reaction step, and the principal products of the reaction do not contain aromatic ring structure, and the degree of deoxidation depends on the reaction temperature. The reaction product is mainly methoxylcyclohexane, and the selectivity of cyclohexane is only 20.3% at 200 ℃.It was found that the selectivity of cyclohexane increases gradually as the reaction temperature rises. The major products are almost all saturated alkanes without oxygen, and the selectivity of cyclohexane reaches 100% with a temperature of 240 ℃

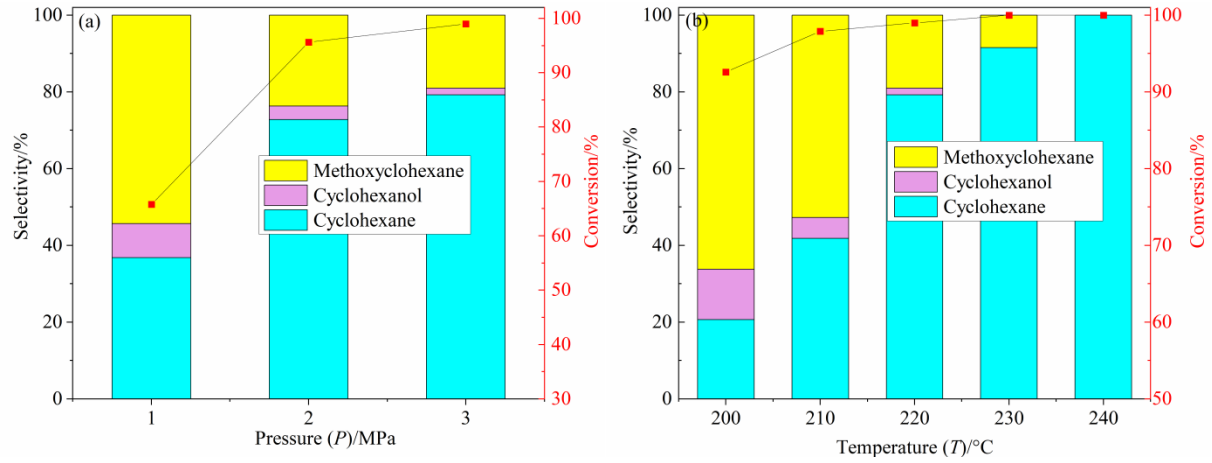

Fig.8. (a)Effect of reaction temperature on HDO of anisole .(b)Effect of reaction pressure on HDO of anisole. （Reaction conditions: (a) 0.1 g $Ni_{0.9}Nb_{0.1}$ catalyst, 13.9 mmol anisole,15 mLC_{12}, 4h, 700 rpm 220℃, (b) 0.1 g $Ni_{0.9}Nb_{0.1}$ catalyst,13.9mmol anisole, 15 mLC_{12}, 3 MPa, 4 h, 700 rpm.）

In order to further understand the variation of reaction products with time, three

different temperatures (200, 220 and 240 ℃) were selected to investigate the variation of reaction products with reaction time from 1 to 6 hours (see Fig.9). At the reaction temperature of 200 ℃, the reaction product was mainly methoxy-cyclohexane. The selectivity of methoxy-cyclohexane increased along with the prolonging of reaction time, while the selectivity of cyclohexane was low, indicating that the hydrogenation of anisole mainly occurred at a lower temperature. When the reaction temperature was 220 ℃, the selectivity of methoxy-cyclohexane rose at the beginning and then declines with increasing the reaction time, and the selectivity of cyclohexane was gradually increased. The demethylation and dehydration of methoxy-cyclohexane were accelerated with rising the reaction temperature [80]. The selectivity of cyclohexane reached 80% at 240 ℃ and 1 h, and no cyclohexanol was detected. Anisole was almost complete to cyclohexane when the reaction time reached 4 h. It shows that at a higher temperature, the deoxidation reaction rate was faster, that is, the hydrogenation of anisol into methoxycyclohexane, immediately deoxidation to cyclohexane.

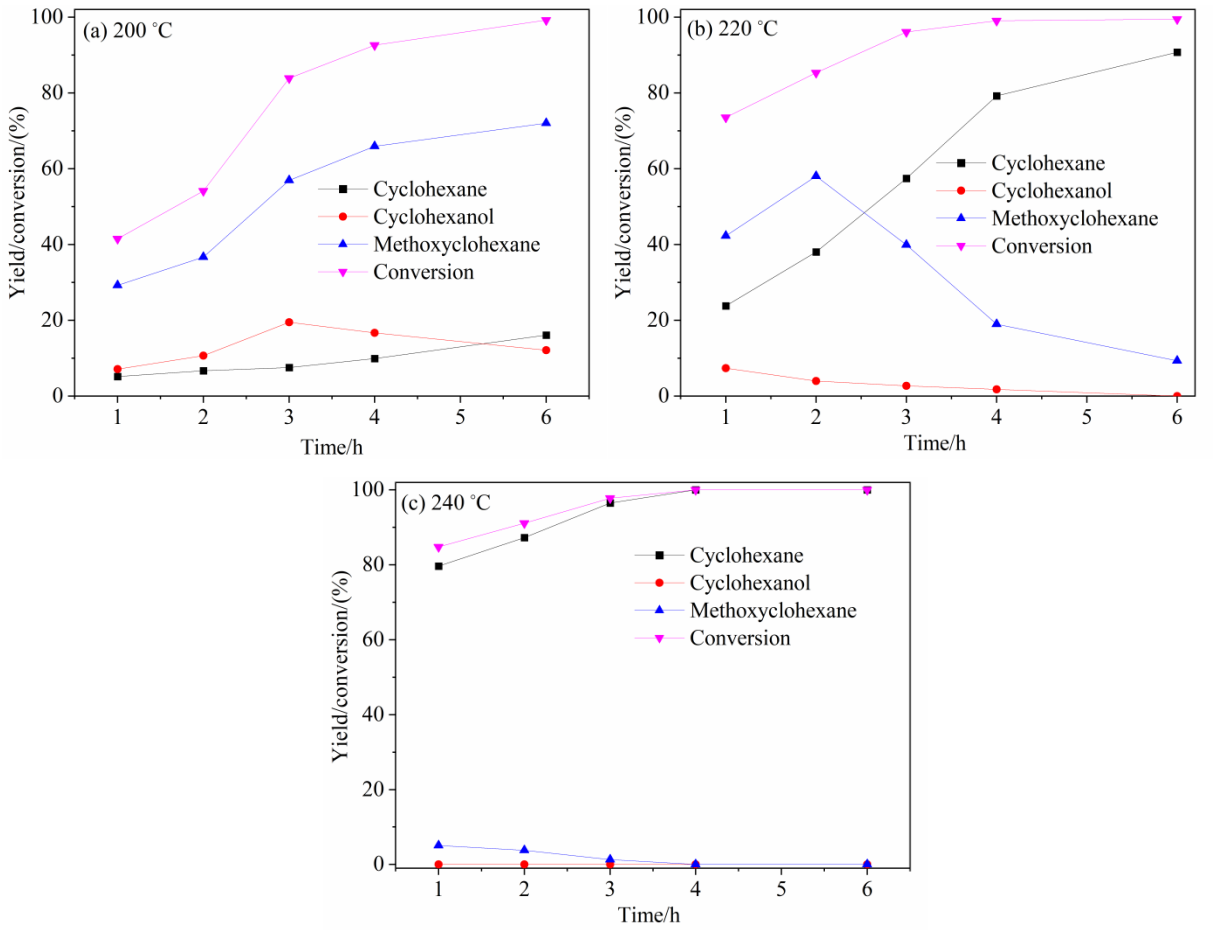

Fig.9. Effect of reaction time on HDO of anisole over $Ni_{0.9}Nb_{0.1}$ catalyst (a.200, b.220，and c.240℃) (Reaction conditions: 0.1 g $Ni_{0.9}Nb_{0.1}$ catalyst, 13.9 mmol anisole, 15 mLC_{12}, 4 h, and 700 rpm).

The amount of catalyst is also an important factor to be considered [81-84]. The influence of $Ni_{0.9}Nb_{0.1}$ catalyst dosage on the reaction process was studied through varying the dosage from 0.04 to 0.12 g. Fig.10 displays the comparison of the conversion of anisole and selectivity of cyclohexane data. The result indicates that the conversion rate of anisole and selectivity of cyclohexane were increased observably (from less than 40% to more than 99%) with the increase of amount of catalyst. When the amount of $Ni_{0.9}Nb_{0.1}$ catalyst was increased to 0.12 g, the reactant conversion rate and selectivity of products selectivity did not increase. Therefore, the optimal amount of catalyst was 0.10 g.

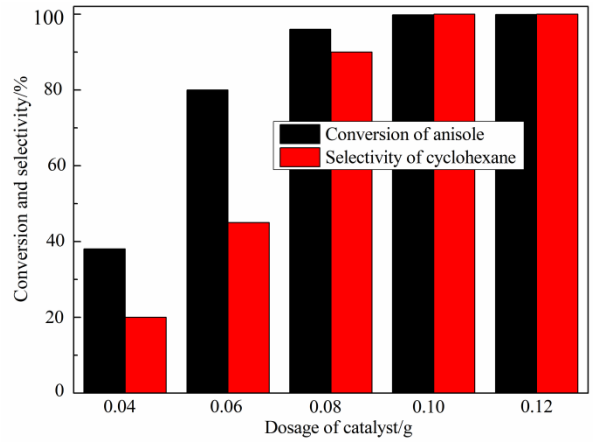

Fig.10. Effect of dosage on HDO of anisole by $Ni_{0.9}Nb_{0.1}$ catalyst.
(Reaction conditions: 13.9 mmol anisole, 15 mLC_{12}, 240℃,4 h, 3 MPa and 700 rpm)

Nanocatalyst must be recyclable and stable in the industrial applications [85-86]. Therefore, the reusability of the catalyst should also be considered. The reusability performance of the $Ni_{0.9}Nb_{0.1}$ catalyst was tested under optimum reaction conditions, as shown in Fig.11. The catalyst was regenerated by centrifugation, ethanol washing and drying after the reaction, and used in the next test under the same reaction conditions. The data listed revealed that the conversion rate of anisole remained almost unchanged during six successive runs, and the selectivity of cyclohexane was gradually decreased from 99.8 to 76%, indicating that the activity of the catalyst decreased slightly but not significantly. Therefore, the nanosphere Ni-Nb_2O_5 composite prepared by sol-gel method is considered to be a promising multiphase catalyst with reusability.

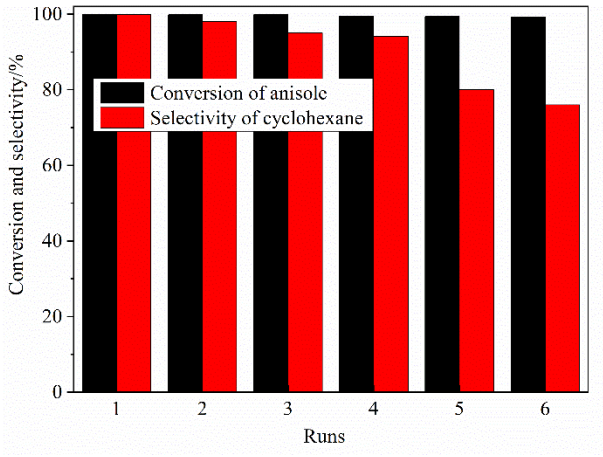

Fig.11. Reusability performance (Reaction conditions:0.1 g $Ni_{0.9}Nb_{0.1}$ catalyst, 13.9 mmol anisole, 15 mLC_{12}, 240℃, 3 MPa, 4h,700 rpm.

In order to find out the reasons for the decrease in activity, XRD and TG analyses were performed on the used catalysts, as shown in Fig.12. It can be seen from Fig.12(a) that the diffraction pattern of $Ni_{0.9}Nb_{0.1}$ catalyst after four cycles is similar to that of fresh nano-catalyst, but the diffraction peaks of Ni and NiO appear after 6 cycles, indicating that part of nickel is oxidized, which may lead to the decrease of catalyst activity. In addition, the mass loss rate of catalyst after 6 cycles was 1.8% higher than that of fresh catalyst (0.9%) according to the TG curve (Fig.12(b)).It may be that a small amount of carbon may be deposited on the surface of the catalyst, which also leads to the decrease of catalyst activity.

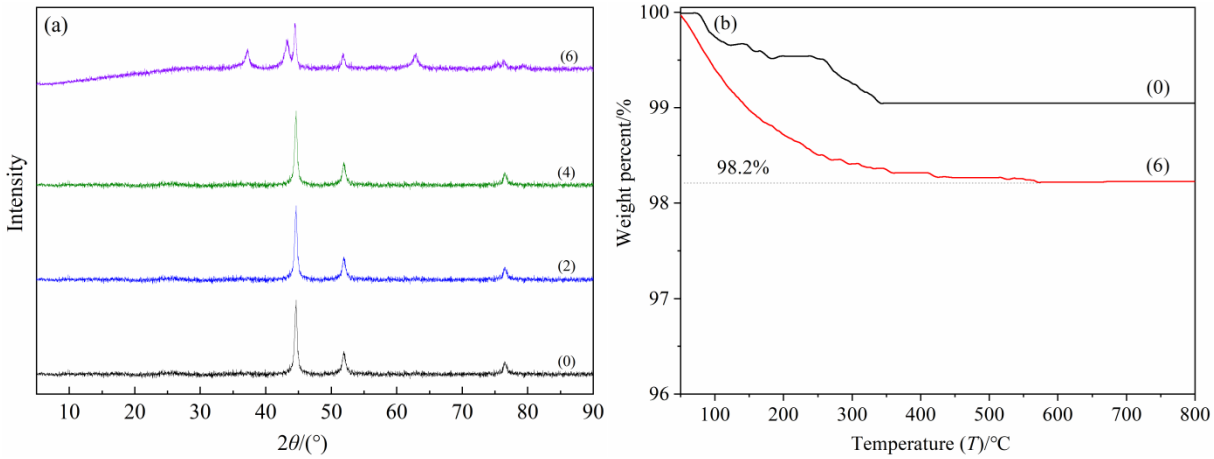

Fig.12. (a)X-ray diffraction (XRD) pattern and (b) TG curveof $Ni_{0.9}Nb_{0.1}$ catalyst (fresh (0), after the second (2), fourth (4), and sixth run reuse (6)).

The possible reaction mechanism of hydrodeoxidation of anisole is proposed as follows according to the experimental data, mainly through three steps:(1) hydrogenation and saturation of aromatic ring in anisole to form methoxycyclohexane; (2) the O-CH_3 bond in methoxy-cyclohexane was hydrogen-dissociated and cyclohexanol was generated after methyl was removed; and (3) through intramolecular dehydration, cyclohexanol deoxidation to produce the final target product cyclohexane. These indicate that the HDO of anisole follows the HYD route [50,87], as shown in Fig.13.

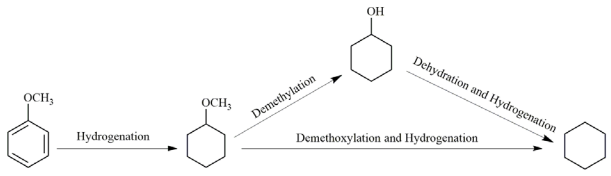

Fig.13. Reaction path of anisole over Ni-Nb_2O_5 catalyst.

4. Conclusion

The nanomaterials with uniform particle size, high dispersibility and high activity were synthesized by the sol-gel method. The Ni-Nb_2O_5 nano-catalysts with different Ni/Nb molar ratios were successfully prepared in this study. The results show that Nb exists as amorphous Nb_2O_5 specie, which can promote the dispersion of Ni components. However, when the content of niobium was high, the Nb-Ni-O mixed phase existed, which reduced the catalytic activity. The size and morphology of Ni grains in catalysts were different due to the difference of Nb/Ni molar ratio. When the molar ratio of Ni/Nb was 0.9/0.1, the surface layer of the sample was porous, with uniform spherical nanoparticles and cracked pores. The specific surface area (170.8 $m^2 \cdot g^{-1}$) and pore volume (0.37 $cm^3 \cdot g^{-1}$) reached the maximum, the average pore size was 4.7 nm, and the catalytic activity was the highest. The $Ni_{0.9}Nb_{0.1}$ catalyst displayed a higher HDO performance for anisole than other catalysts. The selectivity of cyclohexane over the $Ni_{0.9}Nb_{0.1}$ catalyst was about 10 times that of bulk nickel catalyst at 220 ℃, which was mainly attributed to the synergistic effect of metal Ni sites and acid sites provided by the Nb_2O_5 species. The selectivity of cyclohexane increased gradually as the reaction temperature rose. The anisole was almost completely transformed into cyclohexane with a condition of 240 ℃, 3 MPa and 4 h. The catalyst has stable structure and catalytic activity. Based on the liquid products obtained in experiments, the reaction route of anisole HDO following HYD route was proposed.

Acknowledgements

The authors acknowledge Major Science and Technology Project of Yunnan (202102AE090042), National Natural Science Foundation of China (21766016) and the Science and Technology Talent and Platform Program of Yunnan Provincial Science and Technology Department (202005AF150037). The authors acknowledge the financial support of Taif University Researchers Supporting Project (TURSP-2020/27), Taif University, Taif, Saudi Arabia

Declaration of competing interest

There is no conflict of interest recorded for this work.

References

1. Zhang, M., Du, H., Liu, K., Nie, S., Xu, T., Zhang, X., Si, C, Fabrication and applications of cellulose-based nanogenerators. *Adv. Compos. Hybrid Mater*. 4 (4) (2021) 865-884.
2. Hou, C., Wang, B., Murugadoss, V., Vupputuri, S., Chao, Y., Guo, Z., Wang, C., Du, W, Recent advances in Co_3O_4 as anode materials for high-performance lithium-ion batteries. *Eng. Sci.* 11 (2020) 19-30.
3. Zhao, J., Wei, D., Zhang, C., Shao, Q., Murugadoss, V., Guo, Z., Jiang, Q., Yang, X, An overview of oxygen reduction electrocatalysts for rechargeable zinc-air batteries enabled by carbon and carbon composites. *Eng. Sci*. 15 (2021) 1-19.
4. Gao, S., Zhao, X., Fu, Q., Zhang, T., Zhu, J., Hou, F., Ni, J., Zhu, C., Li, T., Wang, Y., Murugadoss, V., Mersal, G., Ibrahim, M., El-Bahy, Z., Huang, M., Guo, Z.， Highly transmitted silver nanowires-SWCNTs conductive flexible film by nested density structure and aluminum-doped zinc oxide capping layer for flexible amorphous silicon solar cells, *J. Mater. Sci. Technol*., 126 (2022) 152-160.
5. Huang, J., Luo, Y., Weng, M., Yu, J., Sun, L., Zeng, H., Liu, Y., Zeng, W., Min, Y., Guo, Z, Advances and applications of phase change materials (PCMs) and PCMs-based technologies. *ES Mater Manuf*. 13 (2021) 23-39.
6. Patil, S. S., Bhat, T. S., Teli, A. M., Beknalkar, S. A., Dhavale, S. B., Faras, M. M., Karanjkar, M. M., Patil, P. S, Hybrid solid state supercapacitors (HSSC's) for high energy & power density: an overview. *Eng. Sci*.12 (2020) 38-51.
7. Sun, Z., Qi, H., Chen, M., Guo, S., Huang, Z., Maganti, S., Murugadoss, V., Huang, M., Guo, Z, Progress in cellulose/carbon nanotube composite flexible electrodes for supercapacitors. Eng. Sci.. 18 (2022) 59-74.
8. Liu, Z., Li, G., Qin, Q., Mi, L., Li, G., Zheng, G., Liu, C., Li, Q., Liu, X, Electrospun PVDF/PAN membrane for pressure sensor and sodium-ion battery separator, *Adv. Compos. Hybrid Mater*. 4 (4) (2021) 1215-1225.
9. Dong, X., Zhao, X., Chen, Y., Wang, C, Investigations about the influence of different carbon matrixes on the electrochemical performance of $Na_3V_2(PO_4)_3$ cathode material for sodium ion batteries, *Adv. Compos. Hybrid Mater.* 4 (4) (2021) 1070-1081.
10. Liu, L., Guo, Z., Yang, J., Wang, S., He, Z., Wang, C, High ion selectivity Aquivion-based hybrid membranes for all vanadium redox flow battery, *Adv. Compos. Hybrid Mater*. 4(3) (2021) 451-458.
11. Ma, Y., Xie, X., Yang, W., Yu, Z., Sun, X., Zhang, Y., Yang, X., Kimura, H., Hou, C., Guo, Z., Du, W, Recent advances in transition metal oxides with different dimensions as electrodes for high-performance supercapacitors, *Adv. Compos. Hybrid Mater*. 4(4) (2021)

906-924.
12. Qu, K., Wang, W., Shi, C., Sun, Z., Qi, H., Shi, J., Yang, S., Huang, Z., Guo, Z, Fungus bran-derived nanoporous carbon with layered structure and rime-like support for enhanced symmetric supercapacitors, *J. Nanostructure. Chem*. 11(4) (2021) 769-784.
13. Zhao, Y., Liu, F., Zhu, K., Maganti, S., Zhao, Z., Bai, P. Three-dimensional printing of the copper sulfate hybrid composites for supercapacitor electrodes with ultra-high areal and volumetric capacitances, *Adv. Compos. Hybrid Mater*., https://doi.org/10.1007/s42114-022-00430-5.
14. Pan, D., Su, F., Liu, C., Guo, Z, Research progress for plastic waste management and manufacture of value-added products, *Adv. Compos. Hybrid Mater*. 3 (4) (2020) 443-461.
15. Guo, L., Zhang, Y., Zheng, J., Shang, L., Shi, Y., Wu, Q., Liu, X., Wang, Y., Shi, L., Shao, Q, Synthesis and characterization of ZnNiCr-layered double hydroxides with high adsorption activities for Cr(VI), *Adv. Compos. Hybrid Mater*. 4(3) (2021)819-829.
16. Cheng, W., Wang, Y., Ge, S., Ding, X., Cui, Z., Shao, Q.: One-step microwave hydrothermal preparation of Cd/Zr-bimetallic metal–organic frameworks for enhanced photochemical properties, *Adv. Compos. Hybrid Mater*. 4(1) (2021) 150-161.
17. Ouyang, L., Huang, W., Huang, M., Qiu, B. Polyaniline improves granulation and stability of aerobic granular sludge, Adv. Compos. Hybrid Mater., 2022, https://doi.org/10.1007/s42 114-022-00450-1
18. Moradi, O., Madanpisheh, M. A., Moghaddas, M, Synthesis of GO/HEMA, GO/HEMA/TiO_2, and GO/Fe_3O_4/HEMA as novel nanocomposites and their dye removal ability, *Adv. Compos. Hybrid Mater*. 4(4) (2021)1185-1204.
19. Ahmadi, S. A. R., Kalaee, M. R., Moradi, O., Nosratinia, F., Abdouss, M, Core–shell activated carbon-ZIF-8 nanomaterials for the removal of tetracycline from polluted aqueous solution, *Adv. Compos. Hybrid Mater*. 4(4) (2021) 1384-1397.
20. Jing, C., Zhang, Y., Zheng, J., Ge, S. et al. In-situ constructing visible light CdS/Cd-MOF photocatalyst with enhanced photodegradation of methylene blue, *Particuology*. 69 (2022) 111-122.
21. Zhang, F., Lian, M., Alhadhrami, A., Huang, M., Li, B., Mersal, G., Ibrahim, M., Xu, M. Laccase immobilized on functionalized cellulose nanofiber/alginate composite hydrogel for efficient bisphenol A degradation from polluted water, *Adv. Compos. Hybrid Mater*. in press, https://doi.org/10.1007/s42114-022-00476-5.
22. Yin, C., Wang, C., Hu, Q, Selective removal of As(V) from wastewater with high efficiency by glycine-modified Fe/Zn-layered double hydroxides, *Adv. Compos. Hybrid Mater*. 4(2) (2021) 360-370.
23. Wang, Y., Xie, W., Liu, H., Gu, H, Hyperelastic magnetic reduced graphene oxide three-dimensional framework with superb oil and organic solvent adsorption capability, *Adv. Compos. Hybrid Mater*. 3(4) (2020) 473-484.

24. Sun, Z., Zhang, Y., Guo, S., Shi, J., Shi, C., Qu, K., Qi, H., Huang, Z., Murugadoss, V., Huang, M., Guo, Z., Confining FeNi nanoparticles in biomass-derived carbon for effectively photo-Fenton catalytic reaction for polluted water treatment, *Adv. Compos. Hybrid Mater*. in press, https://doi.org/10.1007/s42114-022-00477-4
25. Liu, C., Huang, Q., Zheng, K., Qin, J., Zhou, D., Wang, J, Impact of lithium salts on the combustion characteristics of electrolyte under diverse pressures, *Energies*. 13(20) (2020) 5373.
26. Xu, D., Huang, G., Guo, L., Chen, Y., Ding, C., Liu, C, Enhancement of catalytic combustion and thermolysis for treating polyethylene plastic waste, *Adv. Compos. Hybrid Mater*. 5 (2022) 113–129.
27. Wang, W., Deng, X., Liu, D., Luo, F., Cheng, H., Cao, T., Li, Y., Deng, Y., Xie, W, Broadband radar-absorbing performance of square-hole structure, *Adv. Compos. Hybrid Mater*. 5 (2022) 525–535.
28. Luo, F., Liu, D., Cao, T., Cheng, H., Kuang, J., Deng, Y., Xie, W, Study on broadband microwave absorbing performance of gradient porous structure, *Adv. Compos. Hybrid Mater*. 4(3) (2021) 591-601.
29. Si, Y., Li, J., Cui, B., ,Tang, D., Yang, L., Murugadoss, V., Maganti, S., Huang, M., Guo, Z., Janus phenol–formaldehyde resin and periodic mesoporous organic silica nanoadsorbent for the removal of heavy metal ions and organic dyes from polluted water, *Adv. Compos. Hybrid Mater*., https://doi.org/10.1007/s42114-022-00446-x.
30. Niu, M., Sui, K., Wu, X., Cao, D., Liu, C, GaAs quantum dot/TiO_2 heterojunction for visible-light photocatalytic hydrogen evolution: promotion of oxygen vacancy, *Adv. Compos. Hybrid Mater*. 5 (2022) 450–46.
31. Hou, H., Pan, Y., Bai, G., Li, Y., Murugadoss, V., Zhao, Y. High-throughput computing for hydrogen transport properties in ε-ZrH_2, *Adv. Compos. Hybrid Mater.,* https://doi.org/ 10.1007/s42114-022-00454-x.
32. Liu, C., Xu, D., Weng, J., Zhou, S., Li, W., Wan, Y., Jiang, S., Zhou, D., Wang, J., Huang, Q, Phase change materials application in battery thermal management system: A review, *Materials*. 13 (20) (2020) 4622.
33. Liu, F., Zhao, Y., Hou, H., Zhao, Y., Wang, Z., Huang, Z, Synthesis of silicon-based nanosheets decorated with Pd/Li particles with enhanced hydrogen storage properties, *Adv. Compos. Hybrid Mater*. 4(4) (2021) 1343-1353.
34. Hu, H., Ding, F., Ding, H., Liu, J., Xiao, M., Meng, Y., Sun, L, Sulfonated poly(fluorenyl ether ketone)/sulfonated α-zirconium phosphate nanocomposite membranes for proton exchange membrane fuel cells, *Adv. Compos. Hybrid Mater*. 3(4) (2020) 498-507.
35. Ding, F., Hu, H., Ding, H., Liu, J., Chen, Y., Xiao, M., Meng, Y., Sun, L, Sulfonated poly(fluorene ether ketone) (SPFEK)/α-zirconium phosphate (ZrP) nanocomposite membranes for fuel cell applications, *Adv. Compos. Hybrid Mater*. 3 (4) (2020) 546-550.

36. Qu, L., Jiang, X., Zhang, Z., Zhang, X.-g., Song, G.-y., Wang, H.-l., Yuan, Y.-p., Chang, Y.-l.: A review of hydrodeoxygenation of bio-oil: model compounds, catalysts, and equipment, *Green Chem*. 23 (23) (2021) 9348-9376.
37. Deng, Z., Deng, Q., Wang, L., Xiang, P., Lin, J., Murugadoss, V., Song, G, Modifying coconut shell activated carbon for improved purification of benzene from volatile organic waste gas, *Adv. Compos. Hybrid Mater*. 4 (3) (2021) 751-760.
38. Zhu, E.-Q., Xu, G.-F., Ye, X.-Y., Yang, J., Yang, H.-Y., Wang, D.-W., Shi, Z.-J., Deng, J, Preparation and characterization of hydrothermally pretreated bamboo powder with improved thermoplasticity by propargyl bromide modification in a heterogeneous system, *Adv. Compos. Hybrid Mater*. 4 (4) (2021) 1059-1069.
39. Wang, Y., Hu, Y.-J., Hao, X., Peng, P., Shi, J.-Y., Peng, F., Sun, R.-C.: Hydrothermal synthesis and applications of advanced carbonaceous materials from biomass: a review, *Adv. Compos. Hybrid Mater*. 3 (3) (2020) 267-284.
40. Deng, Z., Sun, S., Li, H., Pan, D., Patil, R. R., Guo, Z., Seok, I, Modification of coconut shell-based activated carbon and purification of wastewater, *Adv. Compos. Hybrid Mater*. 4 (1) (2021) 65-73.
41. Yan, J., Niu, Y., Wu, C., Shi, Z., Zhao, P., Naik, N., Mai, X., Yuan, B, Antifungal effect of seven essential oils on bamboo, *Adv. Compos. Hybrid Mater*. 4 (3) (2021) 552-561.
42. Zhu, E.-Q., Xu, G.-F., Sun, S.-F., Yang, J., Yang, H.-Y., Wang, D.-W., Guo, Z.-H., Shi, Z.-J., Deng, J, Rosin acid modification of bamboo powder and thermoplasticity of its products based on hydrothermal pretreatment, *Adv. Compos. Hybrid Mater*. ***4 (3)*** (2021) 584-590.
43. Hong, H., Gao, L., Zheng, Y., Xing, X., Sun, F., Liu, T., Murugadoss, V., Guo, Z., Yang , M., Zhang, H, A path of multi-energy hybrids of concentrating solar energy and carbon fuels for low CO_2 emission, *ES Energy. Environ*. 13 (2021) 1-7.
44. Hua, J., Â MarcusÂ BjÃ¶rling, Â MarcusÂ B., Â Rol, Â., LarssonÂ , L., Shi, Y, Friction control of chitosan-Ag hydrogel by silver ion, *ES Mater. Manuf*. 16 (2022) 30-36.
45. Ong, H. C., Chen, W.-H., Singh, Y., Gan, Y. Y., Chen, C.-Y., Show, P. L, A state-of-the-art review on thermochemical conversion of biomass for biofuel production: A TG-FTIR approach, *Energy Convers. Manage*. 209 (2020) 112634.
46. Mu, L., Dong, Y., Li, L., Gu, X., Shi, Y, Achieving high value utilization of bio-oil from lignin targeting for advanced lubrication, *ES Mater. Manuf*. 11 (2021) 72-80.
47. Corma, A., Iborra, S., Velty, A, Chemical routes for the transformation of biomass into chemicals, *Chem. Rev*. 107 (6) (2007) 2411-2502.
48. Mortensen, P. M., Grunwaldt, J. D., Jensen, P. A., Knudsen, K. G., Jensen, A. D, A review of catalytic upgrading of bio-oil to engine fuels, *Appl. Catal. A*. 407 (1-2) (2011) 1-19.
49. Gu, Y., Pan, Z., Zhang, H., Zhu, J., Yuan, B., Pan, D., Wu, C., Dong, B., Guo, Z, Synthesis of high performance diesel oxidation catalyst using novel mesoporous AlLaZrTiOx mixed oxides by a modified sol-gel method, *Adv. Compos. Hybrid Mater*. 3 (4) (2020) 583-593.

50. Yue, X., Zhang, L., Sun, L., Gao, S., Gao, W., Cheng, X., Shang, N., Gao, Y., Wang, C, Highly efficient hydrodeoxygenation of lignin-derivatives over Ni-based catalyst, *Appl. Catal. B*. 293 (2021) 120243.
51. Nesterov, N. S., Smirnov, A. A., Pakharukova, V. P., Yakovlev, V. A., Martyanov, O. N, Advanced green approaches for the synthesis of NiCu-containing catalysts for the hydrodeoxygenation of anisole, *Catal. Today*. 379 (2021) 262-271.
52. Saidi, M., Safaripour, M, Aqueous phase hydrodeoxygenation of anisole as a pyrolysis lignin-derived bio-oil by ether-functionalized ionic polymer-stabilized Ni-Mo nanocatalyst. Sustain, *Energy Technol. Assess*. 49 (2022) 101770.
53. Taghvaei, H., Moaddeli, A., Khalafi-Nezhad, A., Iulianelli, A, Catalytic hydrodeoxygenation of lignin pyrolytic-oil over Ni catalysts supported on spherical Al-MCM-41 nanoparticles: Effect of Si/Al ratio and Ni loading, *Fuel*. 293 (2021) 120493.
54. Xiang, L., Liu, M., Fan, G., Yang, L., Li, F, MoOx-decorated ZrO_2 nanostructures supporting Ru nanoclusters for selective hydrodeoxygenation of anisole to nenzene, *ACS Appl. Nano Mater*. 4 (11) (2021) 12588-12599.
55. Wang, A., Shi, Y., Yang, L., Fan, G., Li, F, Ordered macroporous Co_3O_4-supported Ru nanoparticles: A robust catalyst for efficient hydrodeoxygenation of anisole, *Catal.Commun*. 153 (2021) 106302.
56. Yan, P., Kennedy, E., Stockenhuber, M, Natural zeolite supported Ni catalysts for hydrodeoxygenation of anisole, *Green Chem*. 23 (13) (2021) 4673-4684.
57. Zhang, Y., Fan, G., Yang, L., Zheng, L., Li, F, Cooperative effects between Ni-Mo alloy sites and defective structures over hierarchical Ni-Mo bimetallic catalysts enable the enhanced hydrodeoxygenation activity, *ACS Sustain. Chem*. Eng. 9 (34) (2021) 11604-11615.
58. Li, X., Chen, L., Chen, G., Zhang, J., Liu, J, The relationship between acidity, dispersion of nickel, and performance of Ni/Al-SBA-15 catalyst on eugenol hydrodeoxygenation, *Renew. Energy*. 149 (2020) 609-616.
59. Yang, Y., Liu, X., Xu, Y., Gao, X., Dai, Y., Tang, Y, Palladium-Incorporated α-MoC mesoporous composites for enhanced direct hydrodeoxygenation of anisole, *Catalysts*. 11 (3) (2021) 370.
60. Yu, Z., Yao, Y., Wang, Y., Li, Y., Sun, Z., Liu, Y.-Y., Shi, C., Liu, J., Wang, W., Wang, A, A bifunctional Ni_3P/γ-Al_2O_3 catalyst prepared by electroless plating for the hydrodeoxygenation of phenol, *J Catal*. 396 (2021) 324-332.
61. Yan, P., Kennedy, E., Stockenhuber, M, Hydrodeoxygenation of guaiacol over BEA supported bimetallic Ni-Fe catalysts with varied impregnation sequence, *J. Catal*. 404 (2021) 1-11.
62. Saidi, M., Moradi, P., Catalytic hydrotreatment of lignin-derived pyrolysis bio-oils using

Cu/γ-Al_2O_3 catalyst: Reaction network development and kinetic study of anisole upgrading, I*nt. J. Energy Res*. 45 (6) (2021) 8267-8284.
63. Aqsha, A., Katta, L., Tijani, M. M., de Oliveira, C. F., Mahinpey, N.: Investigation of catalytic hydrodeoxygenation of anisole as bio-oil model compound over Ni-Mo/TiO_2 and Ni-V/TiO_2 catalysts: Synthesis, kinetic, and reaction pathways studies, *Can. J. Chem. Eng.* 99 (5) (2021) 1094-1106.
64. Shao, Y., Xia, Q., Liu, X., Lu, G., Wang, Y, Pd/Nb_2O_5/SiO_2 catalyst for the direct hydrodeoxygenation of biomass-related compounds to liquid alkanes under mild conditions, *ChemSusChem*. 8 (10) (2015) 1761-1767.
65. Duan, Y., Zhang, J., Li, D., Deng, D., Ma, L.-F., Yang, Y, Direct conversion of carbohydrates to diol by the combination of niobic acid and a hydrophobic ruthenium catalyst, *RSC Adv*. 7 (42) (2017) 26487-26493.
66. Xi, J., Xia, Q., Shao, Y., Ding, D., Yang, P., Liu, X., Lu, G., Wang, Y, Production of hexane from sorbitol in aqueous medium over Pt/$NbOPO_4$ catalyst, *Appl. Catal. B*. 181 (2016) 699-706.
67. Pham, H. N., Pagan-Torres, Y. J., Serrano-Ruiz, J. C., Wang, D., Dumesic, J. A., Datye, A. K, Improved hydrothermal stability of niobia-supported Pd catalysts, *Appl. Catal. A*. 39**7** (1) (2011) 153-162.
68. Jin, S., Xiao, Z., Chen, X., Wang, L., Guo, J., Zhang, M., Liang, C, Cleavage of lignin-derived 4-O-5 aryl ethers over nickel nanoparticles supported on niobic acid-activated carbon composites, *Ind. Eng. Chem*. Res. 54 (8) (2015) 2302-2310.
69. Rojas, E., Delgado, J. J., Guerrero-Pérez, M. O., Bañares, M. A, Performance of NiO and Ni–Nb–O active phases during the ethane ammoxidation into acetonitrile, *Catal. Sci. Technol*. 3 (12) (2013) 3173-3182.
70. Heracleous, E., Lemonidou, A. A, Ni–Nb–O mixed oxides as highly active and selective catalysts for ethene production via ethane oxidative dehydrogenation. Part I: Characterization and catalytic performance, *J. Catal*. 237 (1) (2006) 162-174.
71. Skoufa, Z., Heracleous, E., Lemonidou, A. A.: Unraveling the contribution of structural phases in Ni–Nb–O mixed oxides in ethane oxidative dehydrogenation, *Catal. Today*. 192 (1) (2012) 169-176.
72. Salagre, P., Fierro, J. L. G., Medina, F., Sueiras, J. E, Characterization of nickel species on several γ-alumina supported nickel samples, *J. Mol. Catal. A-Chem*. 106 (1) (1996) 125-134.
73. Pomeroy, B., Grilc, M., Gyergyek, S., Likozar, B, Catalyst structure-based hydroxymethylfurfural (HMF) hydrogenation mechanisms, activity and selectivity over Ni, *Chem. Eng. J*. 412 (2021) 127553.
74. Rynkowski, J. M., Paryjczak, T., Lenik, M, On the nature of oxidic nickel phases in NiO/γ-Al_2O_3 catalysts, *Appl. Catal. A-Gen*. 106 (1) (1993) 73-82.

679 75. Song, W., He, Y., Lai, S., Lai, W., Yi, X., Yang, W., Jiang, X, Selective hydrodeoxygenation
680 of lignin phenols to alcohols in the aqueous phase over a hierarchical Nb_2O_5-supported Ni
681 catalyst, *Green Chem*. 22 (5) (2020) 1662-1670.
682 76. Niwa, M., Katada, N., Sawa, M., Murakami, Y, Temperature-programmed desorption of
683 ammonia with readsorption based on the derived theoretical equation, *J. Phys. Chem*. 99 (21)
684 (1995) 8812-8816.
685 77. Alonso, D. M., Wettstein, S. G., Dumesic, J. A, Bimetallic catalysts for upgrading of
686 biomass to fuels and chemicals, *Chem. Soc. Rev*. 41 (24) (2012) 8075-8098.

687 78. Nakajima, K., Baba, Y., Noma, R., Kitano, M., N. Kondo, J, Hayashi, S., Hara, M.:
688 $Nb_2O_5 \cdot nH_2O$ as a heterogeneous catalyst with water-tolerant lewis acid stes, *J. Am. Chem.*
689 *Soc*. 133 (12) (2011) 4224-4227.

690 79. Savova, B., Loridant, S., Filkova, D., Millet, J. M. M.: Ni–Nb–O catalysts for ethane
691 oxidative dehydrogenation, *Appl Catal. A-Gen*. 390 (1) (2010) 148-157.
692 80. Zhao, C., He, J., Lemonidou, A. A., Li, X., Lercher, J. A, Aqueous-phase
693 hydrodeoxygenation of bio-derived phenols to cycloalkanes, *J Catal*. 280 (1) (2011) 8-16.
694 81. Rezvani, M. A., Miri, O. F, Synthesis and characterization of PWMn/NiO/PAN nanosphere
695 composite with superior catalytic activity for oxidative desulfurization of real fuel, *Chem.*
696 *Eng. J*. 369 (2019) 775-783.
697 82. Rezvani, M. A., Rahmani, P, Synthesis and characterization of new nanosphere hybrid
698 nanocomposite polyoxometalate@ceramic@polyaniline as a heterogeneous catalyst for
699 oxidative desulfurization of real fuel, *Adv. Powder Technol*. 30 (12) (2019) 3214-3223.

700 83. Rezvani, M. A., Shaterian, M., Aghmasheh, M, Catalytic oxidative desulphurization of
701 gasoline using amphiphilic polyoxometalate@polymer nanocomposite as an efficient,
702 reusable, and green organic–inorganic hybrid catalyst, *Environ. Technol*. 41 (10) (2020)
703 1219-1231.

704 84. Rezvani, M. A., Imani, A, Ultra-deep oxidative desulfurization of real fuels by
705 sandwich-type polyoxometalate immobilized on copper ferrite nanoparticles, $Fe_6W_{18}O_{70} \subset$
706 $CuFe_2O_4$, as an efficient heterogeneous nanocatalyst, *J. Environ. Chem. Eng*. 9 (1) (2021)
707 105009.
708 85. Rezvani, M. A., Afshari, P., Aghmasheh, M, Deep catalytic oxidative desulfurization
709 process catalyzed by TBA-PWFe@NiO@BNT composite material as an efficient and
710 recyclable phase-transfer nanocatalyst, *Mater. Chem. Phys*. 267 (2021) 124662.

711 86. Rezvani, M. A., Hadi, M., Rezvani, H, Synthesis of new nanocomposite based on ceramic
712 and heteropolymolybdate using leaf extract of Aloe vera as a high-performance nanocatalyst
713 to desulfurization of real fuel, *Appl. Organomet. Chem*. 35 (5) (2021)e6176.
714 87. Ambursa, M. M., Juan, J. C., Yahaya, Y., Taufiq-Yap, Y. H., Lin, Y.-C., Lee, H. V, A review

on catalytic hydrodeoxygenation of lignin to transportation fuels by using nickel-based catalysts, *Renew. Sust. Energ. Rev*. 138 (2021) 110667.